Molecular Therapy
Methods & Clinical Development
Original Article

DNAJC14 Ameliorates Inner Ear Degeneration in the DFNB4 Mouse Model

Hye Ji Choi,[1,8] Hyun Jae Lee,[1,8] Jin Young Choi,[2] Ik Hyun Jeon,[3] Byunghwa Noh,[1] Sushil Devkota,[4] Han-Woong Lee,[5] Seong Kug Eo,[2] Jae Young Choi,[1] Min Goo Lee,[6,7] and Jinsei Jung[1]

[1]Department of Otorhinolaryngology, Yonsei University College of Medicine, Seoul 120-752, Republic of Korea; [2]Department of Microbiology, College of Veterinary Medicine, Chonbuk National University, Iksan City 54596, Republic of Korea; [3]Department of Ophthalmology, Yonsei University College of Medicine, Seoul 120-752, Republic of Korea; [4]Section of Cell and Developmental Biology, University of California San Diego, 9500 Gilman Drive, La Jolla, CA 92093, USA; [5]Department of Biochemistry, College of Life Science and Biotechnology, Laboratory Animal Research Center, Yonsei University, Seoul 03722, Republic of Korea; [6]Department of Pharmacology, Yonsei University College of Medicine, Seoul 120-752, Republic of Korea; [7]Brain Korea 21 Project for Medical Sciences, Yonsei University College of Medicine, Seoul 120-752, Republic of Korea

The His723Arg (H723R) mutation in *SLC26A4*, encoding pendrin, is the most prevalent mutation in East Asia, resulting in DFNB4, an autosomal recessive type of genetic hearing loss. Although the main pathological mechanism of H723R was identified as a protein-folding defect in pendrin, there is still no curative treatment for associated hearing loss. Here, we show that H723R-pendrin expression and activity are rescued by activation of the chaperonin DNAJC14. *In vitro*, DNAJC14 was activated via Japanese encephalitis virus (JEV) inoculation, and toxin-attenuated JEV rescued the surface expression and anion exchange activity of H723R-pendrin. Human H723R-pendrin transgenic mice (hH723R Tg) were established in a mouse *slc26a4* knockout background, in which only hH723R-pendrin was expressed in the inner ear (Pax2-Cre dependent) to mimic human DFNB4 pathology. Crossing hH723R Tg with DNAJC14-overexpressing mice resulted in reduced cochlear hydrops and more preserved outer hair cells in the cochlea compared to those in hH723R Tg mice. Furthermore, the stria vascularis and spiral ligament were thicker and KCNJ10 expression was increased with DNAJC14 overexpression; however, hearing function and enlarged endolymphatic hydrops were not recovered. These results indicate that DNAJC14 overexpression ameliorates the cochlear degeneration caused by misfolded pendrin and might be a potential therapeutic target for DFNB4.

INTRODUCTION

SLC26A4 encodes pendrin protein, which is an anion exchanger in the inner ear.[1–3] Mutations in *SLC26A4* cause non-syndromic, autosomal recessive hearing loss (DFNB4), which is the most common cause of congenital deafness in east and south Asia.[4–9] In Korea, the allele frequency of the major variants of *SLC26A4* that cause DFNB4 is very high, specifically as much as approximately 0.7%, upon referring to the gnomAD database (http://gnomad.broadinstitute.org/). DFNB4 results in congenital, fluctuating, progressive, and severe-to-profound sensorineural hearing loss.[10] Vestibular functions are also impaired and linked to hearing loss in patients with DFNB4.[11] Most patients with DFNB4 have congenital and severe hearing loss and, thus, undergo cochlear implantation and require hearing rehabilitation. Although residual hearing is often observed at an early age, there is a limited window of several years to remedy or prevent hearing loss during the early stage.[12] Unfortunately, no curable treatment options are currently available for the sensorineural hearing loss that occurs with DFNB4.

Among the pathogenic mutations in the protein encoded by *SLC26A4*, p.H723R (His723Arg) in pendrin is the most common among Korean and Japanese populations.[5,13,14] The pathological mechanism of p.H723R is related to protein misfolding, retention in the endoplasmic reticulum (ER), and degradation by ER-associated degradation (ERAD) pathway.[15,16] Recent studies have shown that misfolded proteins can be expressed on the cellular surface via an unconventional secretion pathway comprising Golgi-bypassing trafficking under ER stress.[16–18] Thus, p.H723R-pendrin (H723R-pendrin) can be rescued on the cell surface via this unconventional trafficking pathway, which is mediated by Hsp70 and its co-chaperone DNAJC14. Hsp70 and DNAJC14 then interact with H723R-pendrin and retrieve the misfolded pendrin from the ERAD pathway to deliver it to the cell surface.[16]

DNAJC14 is an ER chaperonin that modulates the cell-surface trafficking of dopamine D1 receptor and SNARE complex-mediated lysosomal trafficking.[19,20] Interestingly, DNAJC14 also modulates RNA replication for viruses of the Flaviviridae family after infection in mammalian cells.[21] This protein is activated by *Flavivirus* infection and is recruited to the virus replication complex, where it mediates viral

Received 27 April 2019; accepted 23 November 2019;
https://doi.org/10.1016/j.omtm.2019.11.019.

[8]These authors contributed equally to this work.

Correspondence: Jinsei Jung, Department of Otorhinolaryngology, Yonsei University College of Medicine, 134 Sinchon-dong, Seodaemun-gu, Seoul 120-752, Korea.
E-mail: jsjung@yuhs.ac

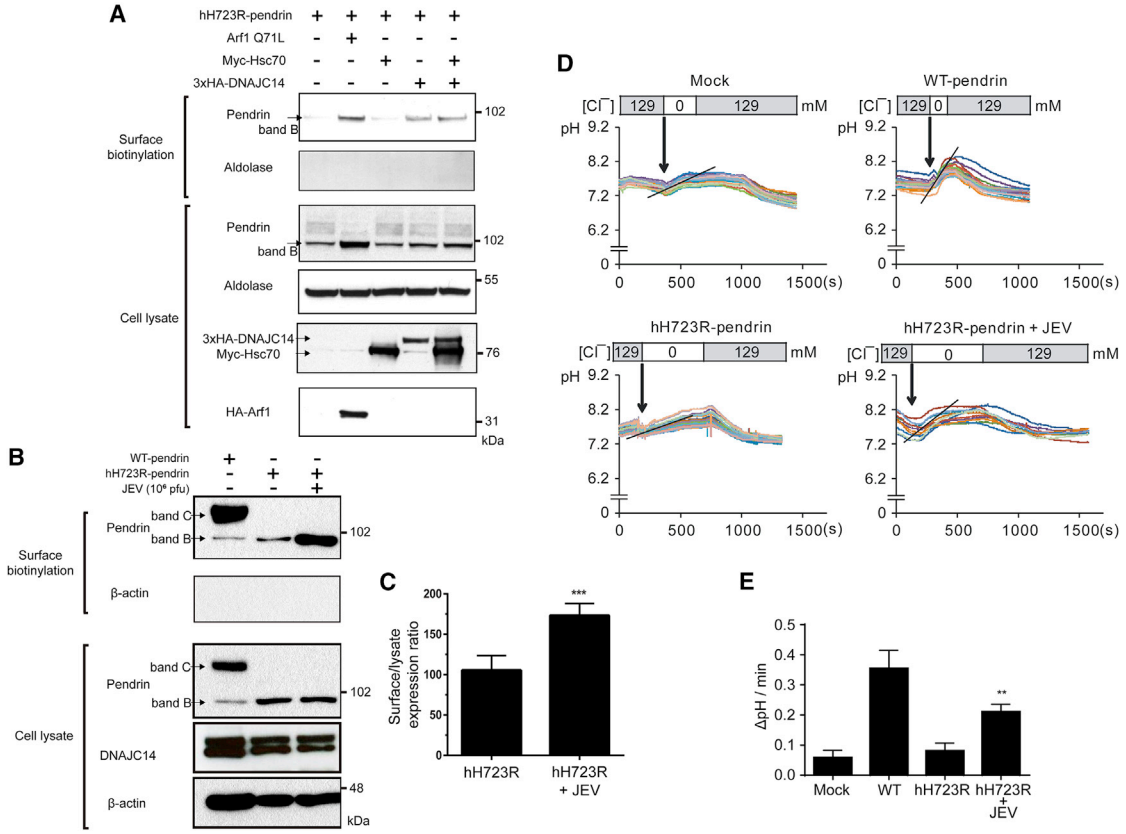

Figure 1. Rescue of hH723R-Pendrin Expression and Function by Japanese Encephalitis Virus (JEV)

(A) Surface biotinylation assays were performed in PANC-1 cells expressing hH723R-pendrin. Blockade of endoplasmic reticulum (ER-to-Golgi traffic via Arf1-Q71L overexpression induced the cell-surface expression of core-glycosylated H723R-pendrin (band B). Overexpression of DNAJC14 (3× HA-tagged) alone or with Hsc70 (Myc-tagged) induced the cell-surface expression of core-glycosylated H723R-pendrin in PANC-1 cells. (B) Surface biotinylation assay in PANC-1 cells transfected with plasmids encoding wild-type (WT)- and hH723R-pendrin after treatment with JEV (10^6 pfu). Band B, ER core-glycosylated immature pendrin; band C, fully glycosylated mature pendrin. The first lane is the positive control cells, in which the band C form of WT-pendrin was expressed on the cell surface. The second lane is the negative control cells, in which the cell-surface band C form of hH723R-pendrin was not expressed and the band B form was weakly expressed. The last lane is cells treated with JEV (10^6 pfu), which induced the cell-surface expression of the band B form of hH723R-pendrin on the cell surface. (C) The surface expression ratio of pendrin (compared to total lysate pendrin) was significantly increased by JEV treatment (10^6 pfu) (n = 8 in each group). ***$p < 0.001$. (D) Cl^-/HCO_3^- exchange activity measured by recording the pH-sensitive fluorescent probe 2′,7′-bis-(2-carboxyethyl)-5-(and-6)-carboxyfluorescein (BCECF) in PANC-1 mock cells and in WT- and hH723R-pendrin stably expressing cells, as detailed in the Materials and Methods. (E) The quantitation of multiple experiments showed that the Cl^-/HCO_3^- exchange activity was significantly increased in the cells expressing hH723R-pendrin with JEV (3×10^6 pfu) treatment (n = 6 in each group). **$p < 0.01$.

replication on the ER membranes by affecting viral polyprotein processing through the promotion of protein folding.[21–23] This phenomenon is highly reminiscent of the unconventional trafficking of H723R-pendrin via the Hsp70/DNAJC14 machinery in terms of protein folding and trafficking from the ER to the cell surface.[16] Therefore, we hypothesized that the administration of a *Flavivirus* such as yellow fever virus or Japanese encephalitis virus (JEV) would activate the Hsp70/DNAJC14 machinery to enhance the unconventional trafficking of H723R-pendrin and subsequently rescue the function of pendrin. We tested this hypothesis using an *in vitro* model of JEV-infected human pancreatic cancer cell line (PANC-1) cells expressing H723R-pendrin. Furthermore, we investigated the effect of enhanced DNAJC14 on changes in inner ear histology and auditory function in human p.H723R-pendrin (hH723R) transgenic (Tg) mice and DNAJC14-overexpressing mice, mimicking the pathology of hearing loss associated with human DFNB4.

RESULTS

JEV Rescues the Expression and Function of hH723R-Pendrin

We previously reported that H723R-pendrin has a folding defect and is rescued by DNAJC14 overexpression.[16] Here, we also observed that the surface expression of hH723R-pendrin was increased in a DNAJC14-dependent manner (Figure 1A). Next, we investigated the effect of JEV on the trafficking of hH723R-pendrin, given that *Flavivirus* species such as JEV activate DNAJC14. In line with our hypothesis, when stable PANC-1 cells expressing hH723R-pendrin were treated with toxin-attenuated JEV, the surface expression of hH723R-pendrin significantly increased, whereas the levels of

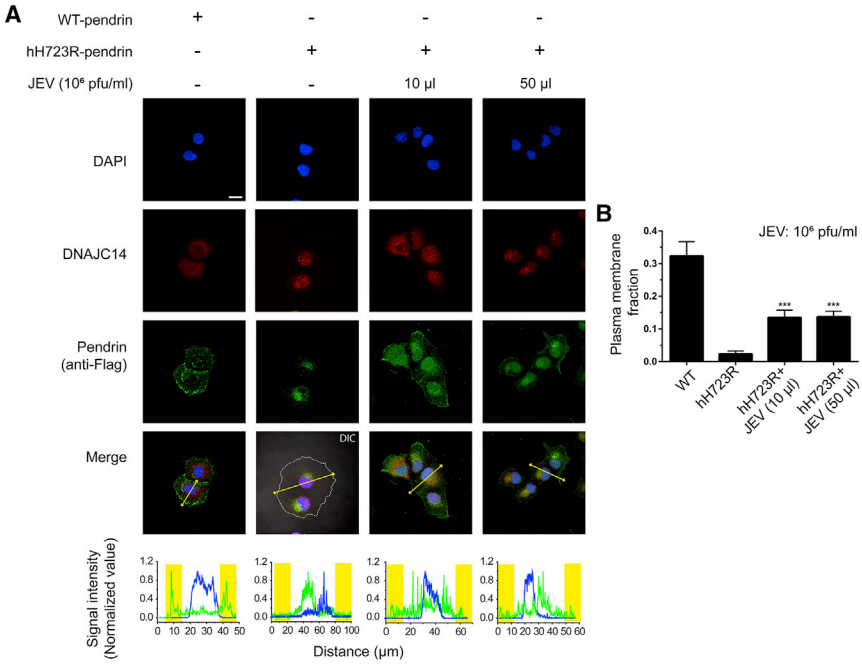

Figure 2. Japanese Encephalitis Virus (JEV) Restores the Expression of Cell-Surface hH723R-Pendrin

Cell-surface pendrin expression was examined in PANC-1 cells with immunostaining. (A) The cells were stained for pendrin (anti-Flag, green) and co-stained for DNAJC14 (red). Nuclei were counterstained with DAPI. DIC images were overlapped in the second lane to clarify the boundary of cells (dashed line). Yellow arrow line indicates the axis for the quantification of fluorescence. In the lower panel, fluorescence intensities for pendrin (green) and DAPI (blue) were quantified along the long axis of each cell, where the yellow box refers to the position of the plasma membrane. Scale bar, 20 µm. (B) The plasma membrane fraction of pendrin was calculated as fluorescence signals between a distance of 5 µm from the cell membrane-to-total fluorescence signal in the cell. Compared to that in lane 2 (hH723R-pendrin), both groups treated with JEV at different titers (1×10^4 and 5×10^4 pfu) showed increased expression of pendrin in the cell membrane ($n = 4$). ***$p < 0.001$.

hH723R-pendrin and DNAJC14 in the lysate were not changed, indicating improved trafficking efficiency to the membrane surface (Figures 1B and 1C).

We also investigated the anion-exchange activity of pendrin with the treatment of JEV according to changes in the fluorescence curve of the pH-sensitive fluorescent probe 2′,7′-bis-(2-carboxyethyl)-5-(and-6)-carboxyfluorescein (BCECF), as described previously.[14] The pH increased when the extracellular solution was changed from 129 mM Cl^- to 0 mM Cl^-, owing to the influx of extracellular HCO_3^-. Strong Cl^-/HCO_3^- exchange activity was also elicited by transfection with human wild-type (WT)-pendrin but not with hH723R-pendrin. Notably, the compromised anion exchange activity (Cl^-/HCO_3^-) of hH723R-pendrin was significantly increased by JEV treatment (Figures 1D and 1E). The effect of the JEV treatment was also consistent when we measured formate and bicarbonate (HCO_2^-/HCO_3^-) exchange activity (Figures S1A and S1B). Immunostaining showed that hH723R-pendrin was restricted to the ER but that WT-pendrin was well expressed on the cellular surface (Figure 2). With variable amounts of JEV (10 or 50 µL of a 10^6 pfu/mL suspension), the membrane surface fraction of hH723R-pendrin remarkably increased (Figures 2A, lower panel, and 2B). Taken together, these results suggest that JEV treatment, which activates DNAJC14, increases the cell-surface expression and anion-exchange activity of hH723R-pendrin.

DNAJC14 Ameliorates Structural Degeneration in hH723R Tg(+) Mice

To evaluate the pathology of DFNB4 with DNAJC14 activation for potential therapeutic development, the DFNB4 mouse model expressing H723R-pendrin was used. To establish an H723R mouse model with deafness, we first generated H723R knockin in mice (Figure S2A–S2C). However, hearing function in these mice remained normal, and there were no abnormalities in the inner ear (Figures S2D and S2E), consistent with results of a previous study.[24] Thus, we established hH723R Tg mice (strain name, B6-Tg(CMV-SLC26A4^{tm1})1JJ, allele1: H723R (c.2139G >A)) in a mouse *slc26a4* homozygous knockout (*mPDS*$^{-/-}$) (strain name, 129S-Slc26a4^{tm1Egr}/AjgJ) background. The hH723R-flanked transgene (Figure S3A) was designed and inoculated into the embryos of B6 mice, which were then crossed with Pax2-Cre mice to achieve inner ear- and kidney-specific expression of hH723R-pendrin. The hH723R Tg mice were subsequently crossed with *mPDS*$^{-/-}$ mice to only express hH723R in the inner ear and kidney, without the expression of mouse pendrin. As a positive control, we also established human WT-pendrin Tg (hPDS Tg; strain name, B6-Tg(CMV-SLC26A4)0JJ) mice. Western blotting confirmed ectopic expression of WT-pendrin in the kidney and cochlea but not in the liver and intestine (Figure S3B, left panel). In hH723R Tg mice, hH723R-pendrin was identified in the cochlea (Figure S3B, right panel). hPDS Tg mice were underweight, and their lifespan was limited to only 2 months, which might be attributable to the ectopic overexpression of pendrin in the kidneys causing kidney dysfunctions such as electrolyte imbalance.

The auditory brainstem response (ABR) test demonstrated deafness in the hH723R Tg mice, mimicking human DFNB4, whereas the hPDS Tg mice showed normal hearing (Figure S3C). Cochlear histology clearly identified cochlear hydrops in both *mPDS*$^{-/-}$ and hH723R Tg(+);*mPDS*$^{-/-}$ mice, but not in hPDS Tg(+); *mPDS*$^{-/-}$ mice ubiquitously expressing ectopic WT-pendrin in the cochlea (Figure S3D). Based on whole-mount images and surface

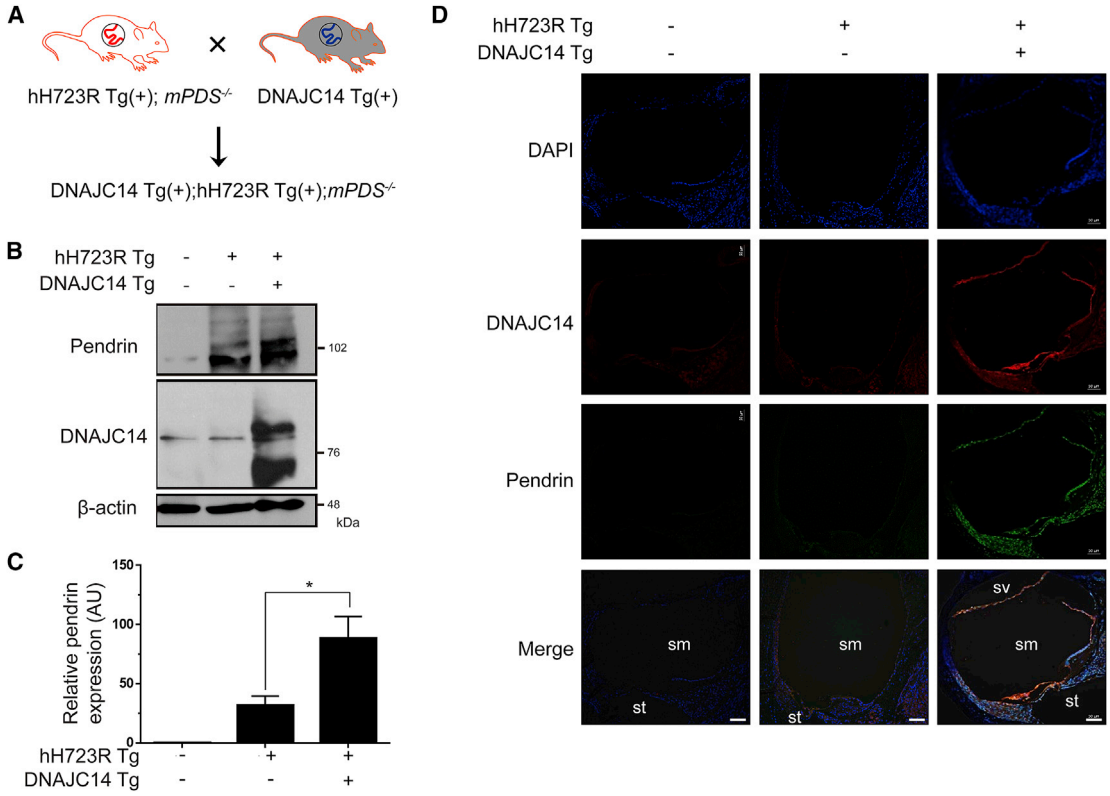

Figure 3. Overexpression of DNAJC14 in hH723R-Pendrin Transgenic Mouse

(A) For activation of DNAJC14 in the established hH723R-pendrin transgenic (hH723R Tg) mouse model, hH723R Tg mice were crossed with Tg mice overexpressing DNAJC14. (B) Based on western blotting of the cochlea, expression of pendrin was increased by overexpressing DNAJC14. (C) Quantification of the density of pendrin is depicted in (AU, arbitrary unit) (n = 4 in each group). *$p < 0.05$. (D) DNAJC14 expression (red) was identified in the DNAJC14 Tg(+);hH723R Tg(+);mPDS(−/−) mice, and the expression of pendrin was increased in most of the cochlear tissue (Pax2-Cre dependent), as shown by immunostaining using the Alexa 488 secondary antibody (green). DAPI (blue) was used for nuclear staining. Scale bar, 100 μm; sm, scala media; st, scala tympani; sv, scala vestibule.

electron microscopy of cochlear hair cells, the outer and inner hair cells were more preserved in hH723R Tg(+);*mPDS*$^{-/-}$ mice than in *mPDS*$^{-/-}$ mice, indicating that the ectopic expression of hH723R in the inner ear was minimally helpful to maintain cochlear structure and function (Figure S3E). Finally, hH723R Tg(+);*mPDS*$^{-/-}$ mice showed enlarged endolymphatic sacs and ducts compared to those in hPDS Tg(+);*mPDS*$^{-/-}$ animals based on computed tomogram sagittal images (Figure S3F). Taken together, we considered that hH723R Tg(+);*mPDS*$^{-/-}$ mice effectively mimic human pathologies associated with DFNB4, such as deafness.

For the activation of DNAJC14, we crossed hH723R Tg(+); *mPDS*$^{-/-}$ mice with Tg mice overexpressing DNAJC14 (DNAJC14 Tg(+); strain name, B6-Tg(CMV-DNAJC14)2JJ) (Figure 3A). Overexpression of DNAJC14 was confirmed in the cochlea, and the expression of hH723R-pendrin was also increased in the cochlea (Figures 3B and 3C). Because the hH723R Tg mouse model is dependent on Pax2-Cre expression, most of the cochlear tissue was positive for ectopic pendrin expression (Figure 3D). With respect to histological changes, the cochlear hydrops was significantly reduced when DNAJC14 was overexpressed in the cochlea (Figures 4A and 4B), and the stria vascularis and spiral ligament in DNAJC14 Tg(+);hH723R Tg(+);*mPDS*$^{-/-}$ mice were more preserved and thicker when compared to those of hH723R Tg mice (Figures 4C–4E). In addition, degeneration of the outer hair cells in hH723R Tg mice was mitigated by the expression of DNAJC14 (Figures 4F and 4G) and KCNJ10, which is important for the generation of endocochlear potential, was more preserved in the stria vascularis with DNAJC14 overexpression (Figures 4H and 4I). Collectively, these results indicate that DNAJC14 ameliorates cochlear degeneration in hH723R Tg mice.

Meanwhile, when we measured the hearing thresholds based on the ABR, DNAJC14 overexpression did not ameliorate hearing function with respect to auditory thresholds in click and frequency-specific stimuli (Figures 5A and 5B). Furthermore, we observed that the ectopic expression of hH723R in the endolymphatic duct, endolymphatic sac, and ampulla of the semi-circular canal increased with DNAJC14 overexpression (Figure 5C). However, the enlarged endolymphatic duct and sac were not restored with DNAJC14 overexpression. In addition, the giant otoconia identified in hH723R Tg(+);*mPDS*$^{-/-}$ mice was also observed in DNAJC14

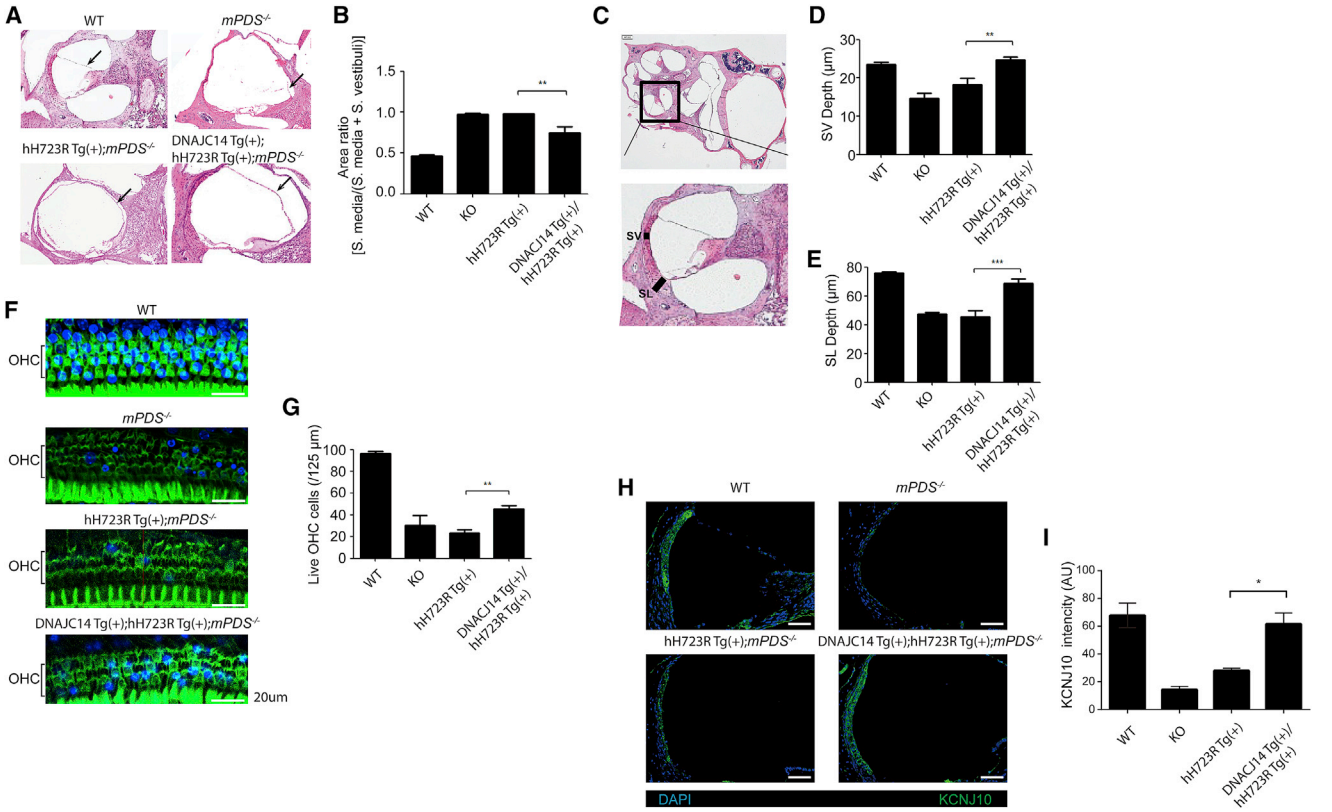

Figure 4. Comparison of Cochlear Histology and KCNJ10 Expression in Mice with Different Genotypes

(A) H&E staining of cochlea from wild-type (WT), *mPDS*$^{-/-}$, hH723R Tg(+);*mPDS*$^{-/-}$, and DNAJC14 Tg(+);hH723R Tg(+);*mPDS*$^{-/-}$ mice at 4–5 weeks of age was performed. (B) Cochlear hydrops in DNAJC14 Tg(+);hH723R Tg(+);*mPDS*$^{-/-}$ mice were significantly reduced (n = 6 mice in each group). **p < 0.01; WT, wild-type; KO, *mPDS*$^{-/-}$. (C) The stria vascularis (SV) and spiral ligament (SL) depth were thicker in DNAJC14 Tg(+);hH723R Tg(+);*mPDS*$^{-/-}$ mice than in hH723R Tg(+);*mPDS*$^{-/-}$ mice. (D) SV depth was statistically compared (n = 6 mice in each group). (E) SL depth was statistically compared (n = 6 mice in each group). (F) Whole-mount of cochlear outer hair cells (OHC) at the middle turn. (G) DNAJC14 expression increased the number of OHCs (n = 6 mice in each group). WT, wild-type; KO, *mPDS*$^{-/-}$. (H) KCNJ10 (green) immunostaining showed increased expression of KCNJ10 in the stria vascularis, implying that the endocochlear potential might have been partially rescued. DAPI (blue) was used for nuclear staining. Scale bar, 100 μm. (I) KCNJ10 fluorescence histogram of multiple area sections of the stria vascularis (n = 3). * p < 0.05.

Tg(+);hH723R Tg(+);*mPDS*$^{-/-}$ mice. These data indicate that DNAJC14 overexpression was not sufficient to ameliorate hearing loss and vestibular malformation, including enlarged vestibular aqueduct and abnormal otoconia formation.

DISCUSSION

Genetic hearing loss is highly prevalent, with an incidence of 1 in 500–1,000 children.[25] More than half of all cases of congenital hearing loss are caused by genetic variants. However, there is still no clinically curative treatment option for patients with genetic hearing loss. Because mutations in *SLC26A4*, encoding pendrin, are the most common cause of deafness in East Asia, it is important to develop effective therapeutics for patients with DFNB4 or Pendred syndrome.

We previously demonstrated that DNAJC14 is the key modulator that rescues the misfolded pendrin proteins from the ERAD and consequently enhances its expression and function.[16] DNAJC14 is an ER chaperonin that plays various physiological roles in mammalian cells, including the trafficking of dopamine D1 receptor and the lysosome function.[19,20] Interestingly, DNAJC14 also appears to play a role in viral RNA replication in mammalian cells infected with *Flavivirus* species such as yellow fever virus and JEV.[21,23] Although the specific functional interaction underlying the mechanism through which DNAJC14 mediates the RNA replication of *Flavivirus* remains unknown, it seems clear that DNAJC14 is activated and rearranged on the ER membrane in response to *Flavivirus* infection. The present study demonstrated that DNAJC14 assists with the proper folding of misfolded pendrin, thereby facilitating its escape from the ER to the membrane surface. Thus, we reasoned that activated DNAJC14 due to *Flavivirus* infection might also promote the protein folding of H723R-pendrin. As expected, we demonstrated that JEV infection increased the cellular surface expression of H723R-pendrin, which was likely related to the promotion of protein folding and rescue from ERAD. This finding suggests the possible application of attenuated *Flavivirus*, as with the

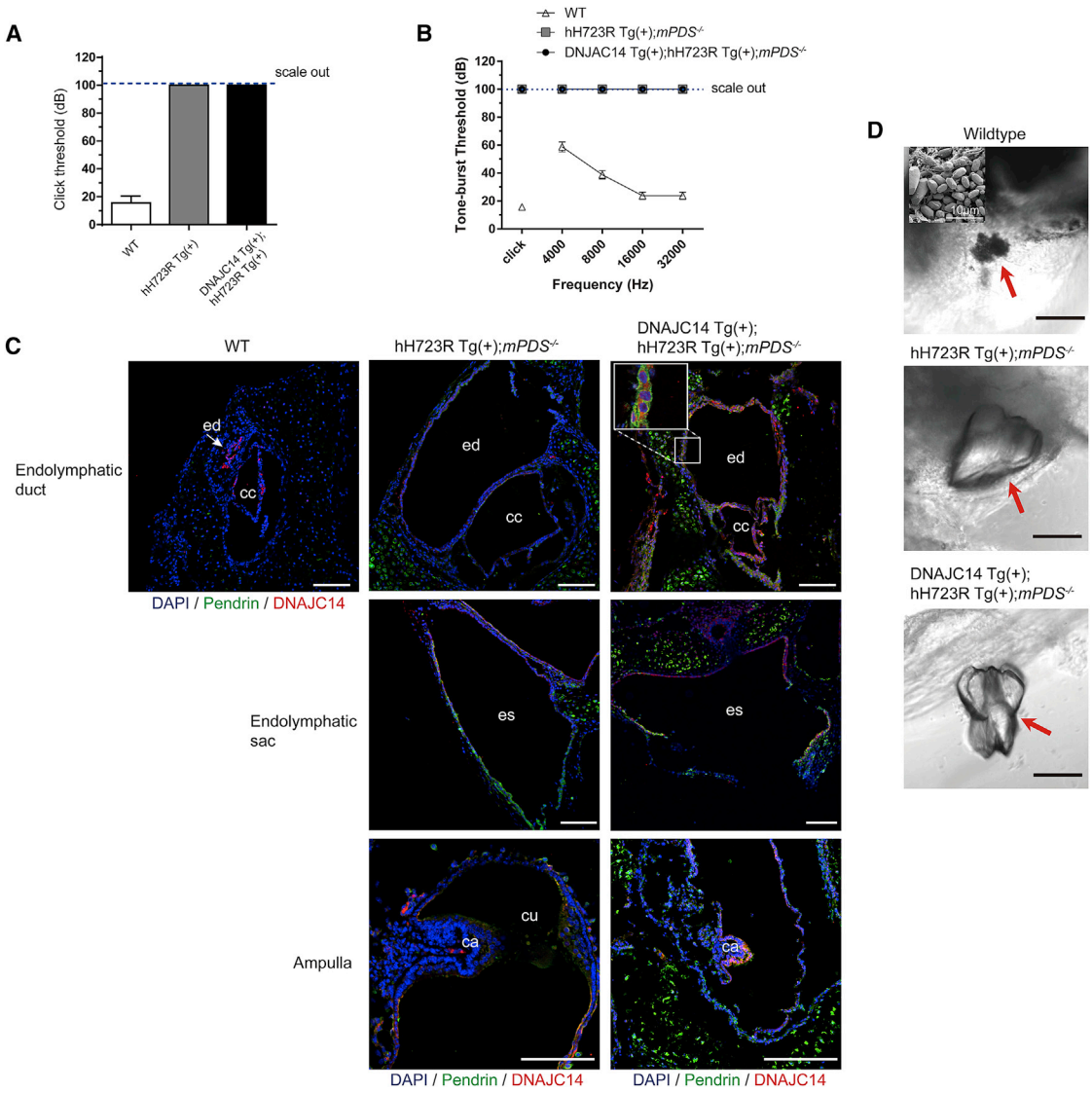

Figure 5. DNAJC14 Overexpression Results in the Insufficient Rescue of Hearing Function and Vestibular Abnormal Morphologies in hH723R Transgenic Mice

(A and B) Auditory brainstem responses by click and tone-burst stimuli were measured in wild-type (WT), hH723R Tg(+);*mPDS*$^{-/-}$, and DNAJC14 Tg(+);hH723R Tg(+);-*mPDS*$^{-/-}$ mice. Auditory threshold was not recovered even if DNAJC14 was overexpressed in hH723R Tg(+);*mPDS*$^{-/-}$ mice based on click (A) and tone-burst (B) stimuli (n = 8 mice in each group). (C) Immunostaining of endolymphatic duct, endolymphatic sac, and ampulla in P0 mice of each strain. hH723R-pendrin (green) was predominantly identified in the epithelial lines (endolymphatic duct, endolymphatic sac, and ampulla) as well as supporting cells, around the endolymphatic duct and common crus (possibly ectopic expression of pendrin depending on CMV promoter) of DNAJC14 Tg(+);hH723R Tg(+);*mPDS*$^{-/-}$ mice. DNAJC14, red; DAPI, blue; ed, endolymphatic duct; cc, common crus; es, endolymphatic sac; ca, crista ampullaris; cu, cupula; white arrow, ed in wild-type; scale bar, 100 μm. (D) Light microscopy and surface electron microscopy were used to observe otoconia morphology (red arrow). Giant otoconia were identified in the macula of hH723R Tg(+);*mPDS*$^{-/-}$ mice (middle), whereas normal-sized otoconia were observed in the macula of WT mice (upper). Giant otoconia were also observed in the macula of DNAJC14 Tg(+);hH723R Tg(+);*mPDS*$^{-/-}$ mice (lower). Scale bar, 100 μm.

strategy used in vaccines, as a therapeutic modality for patients with DFNB4 or Pendred syndrome.

Another important finding of this study is the establishment of a mouse model of H723R mutation-related DFNB4. Although several animal models with mutated pendrin have been reported,[26,27] it has thus far been a challenge to establish a suitable H723R-pendrin mouse model with the human phenotype including deafness.[24] In this study, we successfully established an hH723R-pendrin mouse model with deafness. This model can

thus serve as a useful research tool for drug screening and validation, as well as preclinical trials for hearing preservation drugs that facilitate protein folding.

We also demonstrated that the overexpression of DNAJC14 in the inner ear could ameliorate the histological degeneration caused by the pendrin H723R mutation. Because *slc26a4* knockout results in an enlarged vestibular aqueduct and endolymphatic hydrops in mice, bulging Reissner's membrane in the cochlea due to dilatation of the scala media is typical.[28] This finding was also observed in hH723R Tg(+) mice, which led us to speculate that patients with DFNB4 caused by the H723R mutation might also have cochlear hydrops. Importantly, the size of the cochlear hydrops in hH723R Tg(+) mice was significantly reduced by DNAJC14 overexpression in the inner ear. This indicates that rescued hH723R-pendrin can restore anion exchange (Cl^-/HCO_3^-) activity in the epithelia lining the membranous labyrinth, including the scala media, endolymphatic duct, and sac. We speculated that the partial expressional and functional rescue of hH723R-pendrin makes a difference in the milieu of the endolymph in terms of pH and endocochlear potential. Consequently, outer hair cells, as well as cells in the stria vascularis, might become more stable, and cell survival could increase. However, the protective effect of DNAJC14 on inner ear histology appears to be limited, as hearing loss and hydrops remained and hair cell degeneration occurred over time. Given that DNAJC14 expression was not sufficient to overcome hydrops caused by embryological defects in the hH723R Tg mouse model, hearing function could not be recovered by DNAJC14 in these animals. In addition, the vestibular phenotype, including circling and head tilting, cannot be rescued by the overexpression of DNAJC14 in the inner ear, and it is possible that the mixture of various background strains might affect histological changes in the inner ear. Nevertheless, the hH723R Tg mouse model holds promise for utilization in *in vivo* screens of small molecules that promote protein folding or in gene therapy. In conclusion, we demonstrated that the activation or overexpression of DNAJC14 increases the surface expression and anion-exchange activity of hH723R-pendrin. This finding sheds light on the development of therapeutics for genetic hearing loss caused by *SLC26A4* mutations.

MATERIALS AND METHODS

Cell Culture and Transfection

PANC-1 cells were maintained in DMEM-High Glucose (Lonza, Walkersville, MD, USA) supplemented with 10% fetal bovine serum (FBS) and penicillin (50 IU/mL)/streptomycin (50 μg/mL) at 37°C with 5% CO_2. As previously described for HA-Arf1, pcDNA3-HA-Arf1 and the corresponding empty expression vectors were used for transfection experiments.[17] Human DNAJC14, Hsc70 clones were purchased from Open Biosystems (Lafayette, CO, USA) and subcloned into pCMV-myc or pCMV-Flag plasmids (Clontech, Palo Alto, CA, USA).[16] The expression plasmids for WT- and H723R-pendrin were subcloned into pCMV-Flag plasmids (Clontech, Palo Alto, CA, USA). To establish PANC-1 cells stably expressing WT-pendrin or hH723R-pendrin, each plasmid was transfected into PANC-1 cells using Lipofectamine 2000 reagent (Invitrogen), and puromycin was used to select the transfected cells during 10 passages.

Chemicals and Antibodies

The JEV Beijing-1 strain propagated in a mosquito cell line (C6/36) was kindly supplied by Dr. S.K. Eo (Chonbuk University, Iksan, Korea).[29] Virus stocks (10^6 pfu/mL) were titrated using a conventional plaque assay and stored in aliquots at −80°C until use. The anti-Flag antibody (F3165) was purchased from Sigma-Aldrich (St. Louis, MO, USA). The anti-Myc-Hsc70 (1B5) and anti-DNAJC14 antibody (ab121535) were obtained from Abcam (Cambridge, UK). The anti-pendrin (G-19), anti-aldolase (N-15), anti-3×HA-DNAJC14 (F-7), HA-arf1 (F-7), and anti-β-actin antibody (sc-47778) were from Santa Cruz Biotechnology (Santa Cruz, CA, USA). The anti-KCNJ10 (Kir4.1, Kir1.2) antibody (APC-035) was from Alomone Labs (Jerusalem, Israel).

Surface Biotinylation Assay

The surface proteins were biotinylated with sulfo-NHS-SS-biotin (Pierce) for 30 min before cell lysis. The cells were washed with quenching buffer containing 1% bovine serum albumin (BSA) and then washed three times with phosphate-buffered saline (PBS). After cell lysis with lysis buffer containing 50 mM tris-HCl (pH 8.0), 150 mM NaCl, 1% (v/v) Triton X-100, and complete protease inhibitor mixture (Roche Applied Science, Mannheim, Germany), the lysates were incubated overnight at 4°C with 10% NeutrAvidin beads (Pierce). NeutrAvidin-bound biotinylated proteins were centrifuged and washed three times with PBS and then eluted in 2× sodium dodecyl sulfate (SDS) sample buffer. Protein samples were separated by SDS-polyacrylamide gel electrophoresis. The separated proteins were transferred to a nitrocellulose membrane and blotted with appropriate primary and secondary antibodies. Protein bands were detected by enhanced chemiluminescence.[16]

Measurement of pH_i and Cl^-/HCO_3^- exchange activity

The pH_i in PANC-1 cells, which have minimal intrinsic anion exchange activity, was measured with a pH-sensitive fluorescent probe, BCECF, as described previously.[14] In brief, the pH-sensitive fluorescent probe BCECF was detected in PANC-1 cells transiently transfected WT-pendrin or H723R-pendrin. After JEV treatment for 24 h, PANC-1 cells were incubated with 2 mM BCECF acetoxy-methyl-ester for 15 min and then perfused with an HCO_3^--buffered solution (120 mM NaCl, 5 mM KCl, 1 mM $MgCl_2$, 1 mM $CaCl_2$, 10 mM D-glucose, 5 mM HEPES, and 25 mM $NaHCO_3$ [pH 7.4]). BCECF fluorescence was recorded at the excitation wavelengths of 490 nm and 440 nm at a resolution of 2/s on a recording setup (Carl-Zeiss AxioObserver with Ex-ET436/ET495 and Em-ET540 filters and opti-MOS CCD camera). Cl^-/HCO_3^- exchange activities were estimated from the initial rate of pH increase as a result of Cl^- removal in the HCO_3^--containing buffer (25 mM HCO_3 with 5% CO_2).[16] Cl^--free solutions were prepared by replacing chloride with equimolar gluconate. For $formate^-/HCO_3^-$ exchange activity, Cl^- was replaced with

formate$^-$. The signal of BCECF in cells perforated with nigericin (5 mM) was calibrated with solutions of various pH levels (pH 6.2, 7.2, and 8.2). The buffer capacity of each cell was measured as described previously.[14] Data were analyzed with the Metafluor system (Molecular Devices).

Immunocytochemistry

PANC-1 cells were cultured on coverslips. The cells were permeabilized by incubation in cold ethanol and acetone (1:1) at 20°C for 8 min and blocked by incubation with blocking medium (0.2 mL PBS containing 5% normal donkey serum, 1% BSA, 0.1% gelatin, and 0.001% NaAzide) at 20°C for 1 h to block non-specific binding sites. Subsequently, the cells were stained through incubation with target-specific primary and secondary antibodies (Table S1). Cells were viewed under an LSM780 confocal microscope (Zeiss Laboratories, Jena, Germany).

Animal Experiments

All experimental procedures were approved by Yonsei University Health System Institutional Animal Care and Use Committee (2016-0254). All mice were housed under specific pathogen-free conditions at the animal facility of Yonsei University. All mice were raised at a maximum density of five mice per cage and kept under a 12 h lighting cycle (ambient temperature 18°C–23°C, humidity 40%–60%, 12/12 h light/dark cycle, lights on at 8:00 a.m.). Breeding mice were supplied with nesting materials. All mice were provided with radicidation feed and reverse osmosis water. The cages were ventilated and managed individually with an automatic watering system. All experiments were performed with mice under general anesthesia with tiletamine and zolazepam (100 mg/kg) and xylazine (50 mg/kg) via intraperitoneal injection.

Generation of the hH723R-Pendrin Mouse Model

The mouse pendrin H723R knockin mouse model was generated by Macrogen (Seoul, Korea). The mice were generated using a homologous recombination approach as previously reported.[24] The targeting scheme is described in Figure S2A. The c.2168A>G mutation in exon 19 was targeted for the generation of H723R-PDS mice. Genotype sequencing was performed with the sense primer 5′-AGAACCTGAG ATGGGGATTCATG-3′ and antisense primer 5′-AGCAAATGCCA CATCCGTCAG-3′ (size of amplicons, WT, 842 bp; knockin, 2,126 bp) (Figure S2B).

The human pendrin H723R Tg mouse model was established with a Cre-inducible system, in which the LoxP-STOP-LoxP sequence from pBigT, terminating transcription, was subcloned into the EcoRI site of a pCA GGS vector, and the cDNA fragment encoding human *SLC26A4* (WT or c.2139G>A) was subsequently ligated using XhoI and NotI sites. After confirmation of transgene expression in HEK293T cells with CMV-Cre plasmid expression, the linearized transgene construct was microinjected into pronuclear-stage mouse embryos (C57BL/6N) and transferred to pseudopregnant mice. One Tg founder mouse harboring human *SLC26A4* (WT or c.2139G>A) was identified by PCR amplification of tail genomic DNA and established through germline transmission. Passage-3 hPDS Tg mice were mated with *slc26a4* knockout mice (kindly gifted by Prof. Sung Huhn Kim) to eliminate mouse pendrin. hPDS Tg(+);*mPDS*$^{-/-}$ mice were then mated with Pax2-Cre(+) mice (strain name, B6-Tg(Pax2-cre) 1Akg/Mmnc [stock, MMRRC no. 010569], kindly gifted by Prof. Jinwoong Bok) to generate mice with Pax2-specific expression of human pendrin without mouse pendrin. The final genotype of mice used in the experiments was hPDS Tg(+);Pax2-Cre(+);*mPDS*$^{-/-}$, in which only human pendrin (WT or hH723R) was expressed, but no mouse pendrin was expressed in the inner ear. The genotyping for hPDS Tg, hH723R Tg, Pax2-Cre Tg, and *slc26a4* knockout mice was performed with the following specific primers: human pendrin Tg, fwd 5′-AAC CATGTTCATGCCTTCTTC-3′ and rev 5′-CTAAAGCGCATGCTC CAGA-3′ (amplicon size: 226 bp); Pax2-Cre, fwd 5′-GCCTGCATT ACCGGTCGATGCAACGA-3′ and rev 5′- GTGGCAGATGGCGCG GCAACACCATT-3′ (amplicon size, 700 bp); *slc26a4* KO, fwd 5′-TG CCGATTTCATCGCTGG-3′, rev1 5′-GCATTGTAGTTCTTTTCC AAGTTGG-3′ and Rev2 5′- GGGTGCGGAGAAAGAGGTAATG-3′ (WT, 287 bp; KO, 243 bp).

Inner Ear Western Blotting

Mice at approximately 4–5 weeks of age were anesthetized and then perfused to remove all blood from the entire body. The inner ears of the mice of each genotype were dissected, and then the tissues were chopped and mashed in lysis buffer. After centrifugation of the lysates, the supernatant was used for immunoblotting as described previously herein.

Inner Ear Histology

Tissues from the inner ears of the mice were fixed in 4% paraformaldehyde at 4°C overnight and then washed twice with PBS. Subsequently, the specimens were decalcified in 25% EDTA/PBS for 24 h. Tissues were dehydrated and embedded in paraffin for histology and dissected into segments with the organ of Corti and permeabilized with 0.1% Triton X-100 for whole-mount immunostaining. The paraffin blocks were cut into 5-μm sections using a microtome (Leica Biosystems) and subjected to hematoxylin and eosin (H&E) staining and immunostaining. H&E-stained tissues were examined under a light microscope. For immunostaining, paraffin sections were deparaffinized with xylene, ethanol, and PBS. Thereafter, for antigen retrieval, the sections were incubated in sodium citrate at 95°C for 5 min and then blocked in 10% normal donkey serum for 1 h at room temperature. The tissues were incubated overnight with target-specific primary antibodies at 4°C, washed, and incubated for 1 h at room temperature with the appropriate secondary antibody (Table S1). Finally, the samples were washed and then mounted with mounting solution (Sigma-Aldrich, St. Louis, MO, USA). All images of immunostaining were obtained under a confocal microscope LSM780 (Zeiss Laboratories, Jena, Germany).

Whole-Mount Immunofluorescence

Whole-mount immunofluorescence of cochlea was performed as described previously.[30] In brief, isolated cochleas were obtained

by microdissection. Tissues were fixed by submersion in 4% formaldehyde at 4°C overnight. After washing twice with PBS, the fixed temporal bones were decalcified for 24 h in 10% ethylenediaminetetraacetic acid (EDTA)/PBS. For paraffin sectioning and H&E staining, serial dehydration of the tissues was performed with ethanol and xylene. Then, the tissues were either embedded in paraffin for standard histological examination or dissected into smaller pieces and permeabilized with 0.1% Triton X-100 for whole-mount immunofluorescence. The paraffin blocks were sliced into 5-μm-thick sections in the midmodiolar plane using a microtome (Leica Biosystems, Nußloch, Germany). Deparaffinization was performed on the sections and whole-mounted tissues with a series of washes with xylene, ethanol, and PBS. After incubation in tris-sodium citrate at 95°C for antigen retrieval, the tissues were blocked with 10% donkey serum and incubated with target-specific primary and secondary antibodies at 4°C overnight. The samples were then mounted with mounting solution (Sigma-Aldrich) and viewed under an LSM780 confocal microscope (Zeiss, Jena, Germany).

Auditory Function Test

ABR measurements were recorded as described previously.[30] In brief, tests were conducted using an ABR workstation manufactured by Tucker Davis Technology (Alachua, FL, USA). Properly anesthetized mice were placed on a heating pad (37°C) in a soundproofed chamber. After electrode insertion, acoustic stimuli were applied through a receiver probe. The stimuli included 500 repeated click sounds or tone bursts with a 1-ms rise and fall time and a 5-ms plateau at frequencies of 4, 8, 16, and 32 kHz. The sound intensity began at a 90-dB sound pressure level (SPL) with 5-dB decreasing steps to the auditory threshold.

Micro-computed Tomogram

A custom-built, transmission X-ray microCT scanner of medium energy was used (Model 1076, Skyscan, Aartselaar, Belgium) to obtain images under the conditions of 100 kV of acceleration voltage. After mice were fully anesthetized and fixed, the CT scan was performed. Scanning minimized the changes in the position of the specimen during repeated processes. The 2D images were analyzed using the CTAn (Skyscan, Belgium) computer program.

Scanning Electron Microscopy

Scanning electron microscopy was performed as described previously.[30] Decalcified and fixed cochleas were immersed in 2% glutaraldehyde and paraformaldehyde in 0.1 M PBS, pH 7.4 for 6 h. After washing twice in 0.1 M PBS for 30 min each, tissues were post-fixed with 1% OsO_4, dissolved in 0.1 M PBS for 1.5 h, and dehydrated in an ascending gradual series (50%–100%) of ethanol. Tissues were then treated with isoamyl acetate and subjected to critical point drying with a Leica EM CPD300 (Vienna, Austria). Then they were coated with Platinum (5 nm) using an ion coater (Leica EM ACE600) and examined and photographed with a scanning electron microscope (FE-SEM; Merin, Zeiss).

Statistical Analysis

The results of multiple experiments are presented as the means ± SEM. Statistical comparisons were performed based on analysis of variance followed by the Bonferroni multiple comparison test, where appropriate; $p < 0.05$ was considered statistically significant.

SUPPLEMENTAL INFORMATION

Supplemental Information can be found online at https://doi.org/10.1016/j.omtm.2019.11.019.

AUTHOR CONTRIBUTIONS

Study conception and design, J.J., M.G.L.; Acquisition of data, H.J.C., H.J.L., I.H.J.; Analysis and interpretation of data, J.J, H.J.C., B.N., M.G.L.; Drafting of manuscript, J.J., H.J.C., H.-W.L., S.K.E.; Technical support, S.D., H.-W.L., J.Y.C., S.K.E., J.Y.C.; Essential consulting and reagents, J.Y.C., S.K.E.

CONFLICTS OF INTEREST

The authors declare no competing interests.

ACKNOWLEDGMENTS

This work was supported by the Korean Health Technology R&D Project and the Ministry of Health & Welfare, Republic of Korea (HI16C0142 to J.J.), and by the National Research Foundation of Korea (NRF) grants funded by the Korean government (2017R1D1A1B03030046 to J.J. and 2016M3A9B5941215 to J.Y.C.).

REFERENCES

1. Everett, L.A., Glaser, B., Beck, J.C., Idol, J.R., Buchs, A., Heyman, M., Adawi, F., Hazani, E., Nassir, E., Baxevanis, A.D., et al. (1997). Pendred syndrome is caused by mutations in a putative sulphate transporter gene (PDS). Nat. Genet. *17*, 411–422.
2. Wangemann, P., Nakaya, K., Wu, T., Maganti, R.J., Itza, E.M., Sanneman, J.D., Harbidge, D.G., Billings, S., and Marcus, D.C. (2007). Loss of cochlear HCO3- secretion causes deafness via endolymphatic acidification and inhibition of Ca2+ reabsorption in a Pendred syndrome mouse model. Am. J. Physiol. Renal Physiol. *292*, F1345–F1353.
3. Scott, D.A., Wang, R., Kreman, T.M., Sheffield, V.C., and Karniski, L.P. (1999). The Pendred syndrome gene encodes a chloride-iodide transport protein. Nat. Genet. *21*, 440–443.
4. Park, H.J., Lee, S.J., Jin, H.S., Lee, J.O., Go, S.H., Jang, H.S., Moon, S.K., Lee, S.C., Chun, Y.M., Lee, H.K., et al. (2005). Genetic basis of hearing loss associated with enlarged vestibular aqueducts in Koreans. Clin. Genet. *67*, 160–165.
5. Park, H.J., Shaukat, S., Liu, X.Z., Hahn, S.H., Naz, S., Ghosh, M., Kim, H.N., Moon, S.K., Abe, S., Tukamoto, K., et al. (2003). Origins and frequencies of SLC26A4 (PDS) mutations in east and south Asians: global implications for the epidemiology of deafness. J. Med. Genet. *40*, 242–248.
6. Tsukamoto, K., Suzuki, H., Harada, D., Namba, A., Abe, S., and Usami, S. (2003). Distribution and frequencies of PDS (SLC26A4) mutations in Pendred syndrome and nonsyndromic hearing loss associated with enlarged vestibular aqueduct: a unique spectrum of mutations in Japanese. Eur. J. Hum. Genet. *11*, 916–922.
7. Wang, Q.J., Zhao, Y.L., Rao, S.Q., Guo, Y.F., Yuan, H., Zong, L., Guan, J., Xu, B.C., Wang, D.Y., Han, M.K., et al. (2007). A distinct spectrum of SLC26A4 mutations in patients with enlarged vestibular aqueduct in China. Clin. Genet. *72*, 245–254.
8. Wu, C.C., Yeh, T.H., Chen, P.J., and Hsu, C.J. (2005). Prevalent SLC26A4 mutations in patients with enlarged vestibular aqueduct and/or Mondini dysplasia: a unique spectrum of mutations in Taiwan, including a frequent founder mutation. Laryngoscope *115*, 1060–1064.

9. Dai, P., Yuan, Y., Huang, D., Zhu, X., Yu, F., Kang, D., Yuan, H., Wu, B., Han, D., and Wong, L.J. (2008). Molecular etiology of hearing impairment in Inner Mongolia: mutations in SLC26A4 gene and relevant phenotype analysis. J. Transl. Med. *6*, 74.

10. Pryor, S.P., Madeo, A.C., Reynolds, J.C., Sarlis, N.J., Arnos, K.S., Nance, W.E., Yang, Y., Zalewski, C.K., Brewer, C.C., Butman, J.A., and Griffith, A.J. (2005). SLC26A4/PDS genotype-phenotype correlation in hearing loss with enlargement of the vestibular aqueduct (EVA): evidence that Pendred syndrome and non-syndromic EVA are distinct clinical and genetic entities. J. Med. Genet. *42*, 159–165.

11. Jung, J., Seo, Y.W., Choi, J.Y., and Kim, S.H. (2016). Vestibular function is associated with residual low-frequency hearing loss in patients with bi-allelic mutations in the SLC26A4 gene. Hear. Res. *335*, 33–39.

12. Kim, B.G., Roh, K.J., Park, A.Y., Lee, S.C., Kang, B.S., Seo, Y.J., Lee, J.D., and Choi, J.Y. (2016). Early deterioration of residual hearing in patients with SLC26A4 mutations. Laryngoscope *126*, E286–E291.

13. Dossena, S., Rodighiero, S., Vezzoli, V., Nofziger, C., Salvioni, E., Boccazzi, M., Grabmayer, E., Bottà, G., Meyer, G., Fugazzola, L., et al. (2009). Functional characterization of wild-type and mutated pendrin (SLC26A4), the anion transporter involved in Pendred syndrome. J. Mol. Endocrinol. *43*, 93–103.

14. Lee, H., Jung, J., Shin, J., Song, M., Kim, S., Lee, J.H., Lee, K.A., Shin, S., Kim, U.K., Bok, J., et al. (2014). Correlation between genotype and phenotype in patients with bi-allelic SLC26A4 mutations. Clin. Genet. *86*, 270–275.

15. Yoon, J.S., Park, H.J., Yoo, S.Y., Namkung, W., Jo, M.J., Koo, S.K., Park, H.Y., Lee, W.S., Kim, K.H., and Lee, M.G. (2008). Heterogeneity in the processing defect of SLC26A4 mutants. J. Med. Genet. *45*, 411–419.

16. Jung, J., Kim, J., Roh, S.H., Jun, I., Sampson, R.D., Gee, H.Y., Choi, J.Y., and Lee, M.G. (2016). The HSP70 co-chaperone DNAJC14 targets misfolded pendrin for unconventional protein secretion. Nat. Commun. *7*, 11386.

17. Gee, H.Y., Noh, S.H., Tang, B.L., Kim, K.H., and Lee, M.G. (2011). Rescue of ΔF508-CFTR trafficking via a GRASP-dependent unconventional secretion pathway. Cell *146*, 746–760.

18. Rabouille, C. (2017). Pathways of Unconventional Protein Secretion. Trends Cell Biol. *27*, 230–240.

19. Bermak, J.C., Li, M., Bullock, C., and Zhou, Q.Y. (2001). Regulation of transport of the dopamine D1 receptor by a new membrane-associated ER protein. Nat. Cell Biol. *3*, 492–498.

20. Tchernev, V.T., Mansfield, T.A., Giot, L., Kumar, A.M., Nandabalan, K., Li, Y., Mishra, V.S., Detter, J.C., Rothberg, J.M., Wallace, M.R., et al. (2002). The Chediak-Higashi protein interacts with SNARE complex and signal transduction proteins. Mol. Med. *8*, 56–64.

21. Yi, Z., Sperzel, L., Nürnberger, C., Bredenbeek, P.J., Lubick, K.J., Best, S.M., Stoyanov, C.T., Law, L.M., Yuan, Z., Rice, C.M., and MacDonald, M.R. (2011). Identification and characterization of the host protein DNAJC14 as a broadly active flavivirus replication modulator. PLoS Pathog. *7*, e1001255.

22. Yi, Z., Yuan, Z., Rice, C.M., and MacDonald, M.R. (2012). Flavivirus replication complex assembly revealed by DNAJC14 functional mapping. J. Virol. *86*, 11815–11832.

23. Bozzacco, L., Yi, Z., Andreo, U., Conklin, C.R., Li, M.M., Rice, C.M., and MacDonald, M.R. (2016). Chaperone-Assisted Protein Folding Is Critical for Yellow Fever Virus NS3/4A Cleavage and Replication. J. Virol. *90*, 3212–3228.

24. Lu, Y.C., Wu, C.C., Yang, T.H., Lin, Y.H., Yu, I.S., Lin, S.W., Chang, Q., Lin, X., Wong, J.M., and Hsu, C.J. (2013). Differences in the pathogenicity of the p.H723R mutation of the common deafness-associated SLC26A4 gene in humans and mice. PLoS ONE *8*, e64906.

25. Jung, J., Lee, J.S., Cho, K.J., Yu, S., Yoon, J.H., Yung Gee, H., and Choi, J.Y. (2017). Genetic Predisposition to Sporadic Congenital Hearing Loss in a Pediatric Population. Sci. Rep. *7*, 45973.

26. Lu, Y.C., Wu, C.C., Shen, W.S., Yang, T.H., Yeh, T.H., Chen, P.J., Yu, I.S., Lin, S.W., Wong, J.M., Chang, Q., et al. (2011). Establishment of a knock-in mouse model with the SLC26A4 c.919-2A>G mutation and characterization of its pathology. PLoS ONE *6*, e22150.

27. Choi, B.Y., Kim, H.M., Ito, T., Lee, K.Y., Li, X., Monahan, K., Wen, Y., Wilson, E., Kurima, K., Saunders, T.L., et al. (2011). Mouse model of enlarged vestibular aqueducts defines temporal requirement of Slc26a4 expression for hearing acquisition. J. Clin. Invest. *121*, 4516–4525.

28. Everett, L.A., Belyantseva, I.A., Noben-Trauth, K., Cantos, R., Chen, A., Thakkar, S.I., Hoogstraten-Miller, S.L., Kachar, B., Wu, D.K., and Green, E.D. (2001). Targeted disruption of mouse Pds provides insight about the inner-ear defects encountered in Pendred syndrome. Hum. Mol. Genet. *10*, 153–161.

29. Choi, J.Y., Kim, J.H., Patil, A.M., Kim, S.B., Uyangaa, E., Hossain, F.M.A., and Eo, S.K. (2017). Exacerbation of Japanese Encephalitis by $CD11c^{hi}$ Dendritic Cell Ablation Is Associated with an Imbalance in Regulatory $Foxp3^{+}$ and IL-$17^{+}CD4^{+}$ Th17 Cells and in Ly-$6C^{hi}$ and Ly-$6C^{lo}$ Monocytes. Immune Netw. *17*, 192–200.

30. Jung, J., Yoo, J.E., Choe, Y.H., Park, S.C., Lee, H.J., Lee, H.J., Noh, B., Kim, S.H., Kang, G.Y., Lee, K.M., et al. (2019). Cleaved Cochlin Sequesters Pseudomonas aeruginosa and Activates Innate Immunity in the Inner Ear. Cell Host Microbe *25*, 513–525.e516.

OMTM, Volume *17*

Supplemental Information

DNAJC14 Ameliorates Inner Ear Degeneration in the DFNB4 Mouse Model

Hye Ji Choi, Hyun Jae Lee, Jin Young Choi, Ik Hyun Jeon, Byunghwa Noh, Sushil Devkota, Han-Woong Lee, Seong Kug Eo, Jae Young Choi, Min Goo Lee, and Jinsei Jung

Supplementary Table S1. Antibodies used in this study.

Name	Catalog number (Manufacturer)	Dilution (Use)
Primary Antibody		
Pendrin	G-19 (Santa Cruz)	1:1000 (WB)
Aldolase	N-15 (Santa Cruz)	1:1000 (WB)
3xHA-DNAJC14	F-7 (Santa Cruz)	1:1000 (WB)
Myc-Hsc70	1B5 (Abcam)	1:1000 (WB)
HA-Arf1	F-7 (Santa Cruz)	1:1000 (WB)
anti-pendrin	2-hR2 (ABfrontier)	1:1000 (WB)
anti-β-Actin	sc-47778 (Santa Cruz)	1:2000 (WB)
anti-DNAJC14	ab121535 (Abcam)	1:1000 (WB), 1:200 (IF)
anti-Flag	F3165 (Sigma)	1:2000 (WB), 1:100 (IF)
anti-DAPI	D1306 (Thermo)	1:5000 (ICC), 1:10000 (IHC)
anti-KCNJ10	APC-035 (Alomone Labs)	1:100 (IF)
Secondary Antibody		
anti-mouse, HRP conjugated	G-21040 (Thermo)	1:1000 (WB)
anti-rabbit, HRP conjugated	32460 (Thermo)	1:1000 (WB)
Alexa 488, anti-mouse	A11001 (Invitrogen)	1:1000 (IF)
Alexa 488, anti-rabbit	A11008 (Invitrogen)	1:1000 (IF)
Alexa 568, anti-rabbit	A11036 (Invitrogen)	1:1000 (IF)

IF, immunofluorescence; WB, western blotting; IHC, immunohistochemistry; ICC, immunocytochemistry

Figure S1

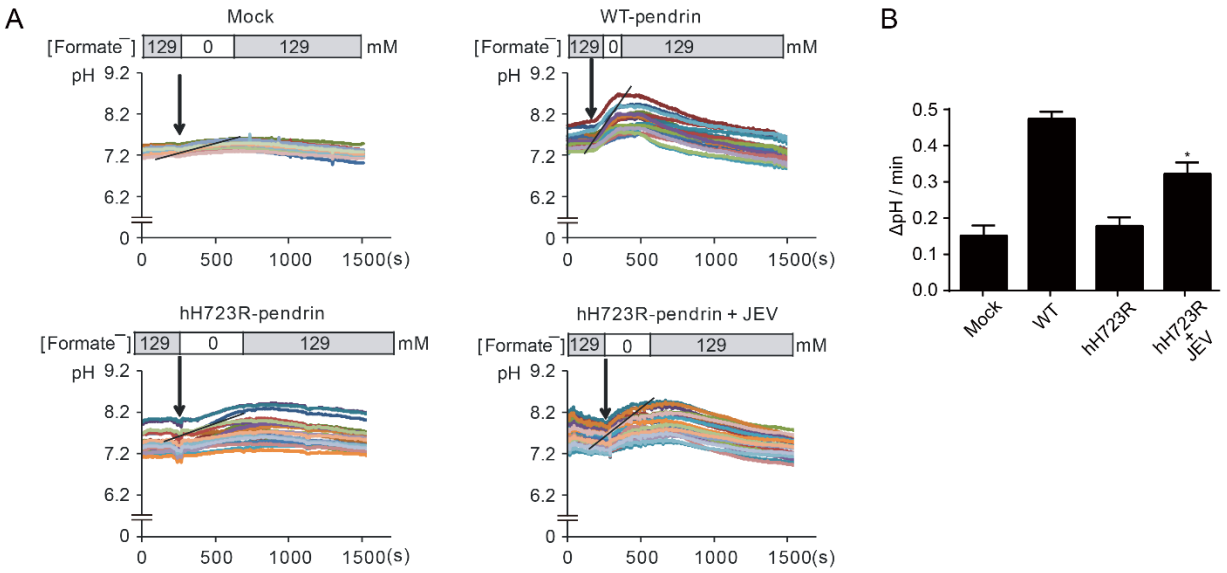

Figure S1. HCO_2^-/HCO_3^- exchange activity by activation of DNAJC14. (A) Formate/Bicarbonate (HCO_2^-/HCO_3^-) exchange activity was measured by recording the pH-sensitive fluorescent probe BCECF in PANC-1 mock cells, and in wild-type (WT)- and human H723R (hH723R)-pendrin stably expressing cells with/without Japanese encephalitis virus (JEV, $3x10^6$ pfu) to activate DNAJC14, as detailed in the Methods. The quantification of multiple experiments is depicted in (B). The HCO_2^-/HCO_3^- exchange activity significantly increased in cells expressing hH723R-pendrin with JEV treatment (n = 4 in each group). *, $p < 0.05$.

Figure S2

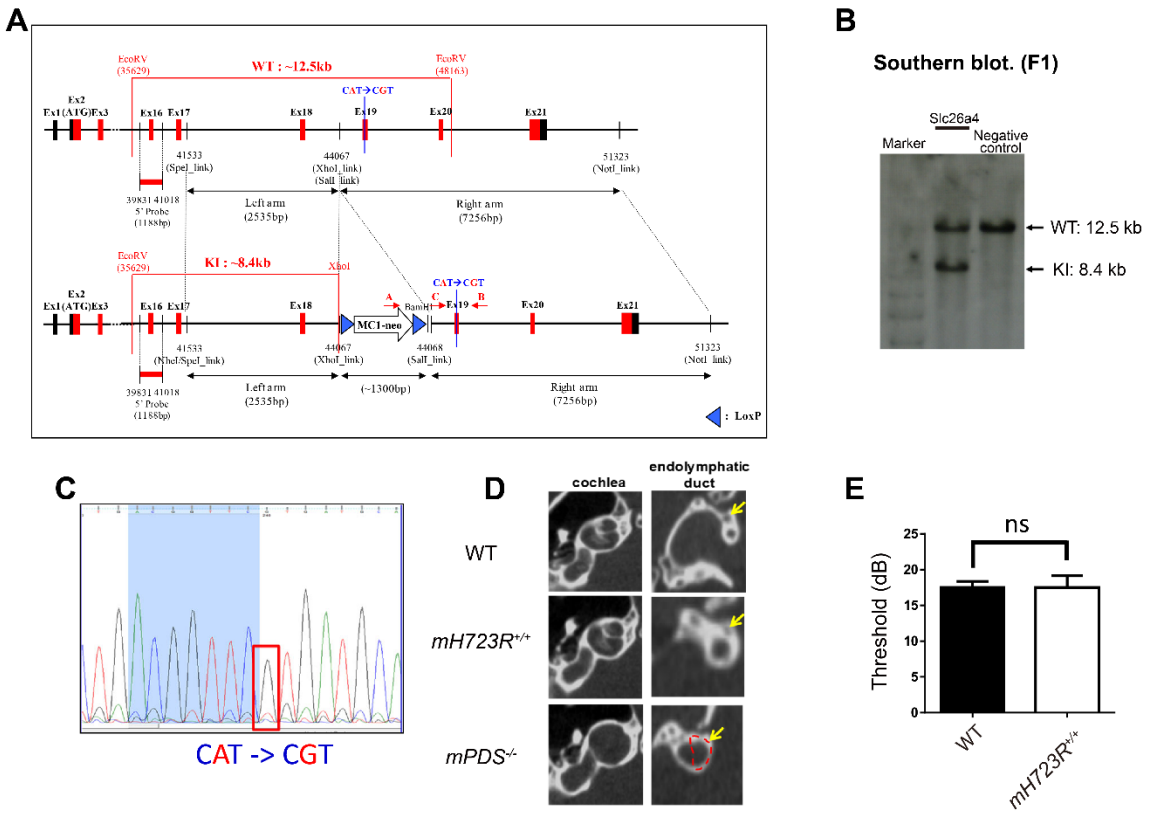

Figure S2. Targeting scheme of the H723R knock-in mouse model. (A) A Bac clone containing *slc26a4* genomic region was used to construct the targeting vector. The expected size of the restriction enzyme fragment of the wild-type (WT) and knock-in (KI) was ~12.5 kb and ~8.4 kb, respectively. The loxP-flanked neomycin resistance gene (neo) was used as a selection marker during embryonic stem (ES) cell culture. (B) The *slc26a4* knock-in (KI) was identified with Southern blotting. (C) Sanger sequencing of the target region revealed that the c.2168A>G point mutation was present in the founder mouse. (D) Micro-computed tomogram of the inner ear. While *slc26a4* knock-out mice (*mPDS*$^{-/-}$) showed a dilated endolymphatic duct and cochlear hydrops, WT and mouse p.H723R KI homozygote [*mH723R*$^{+/+}$] showed normal cochlea and endolymphatic duct. (E) In the auditory brainstem response, both WT and *mH723R*$^{+/+}$ mice showed normal hearing thresholds (n = 13 in each group). ns, not significant.

Figure S3

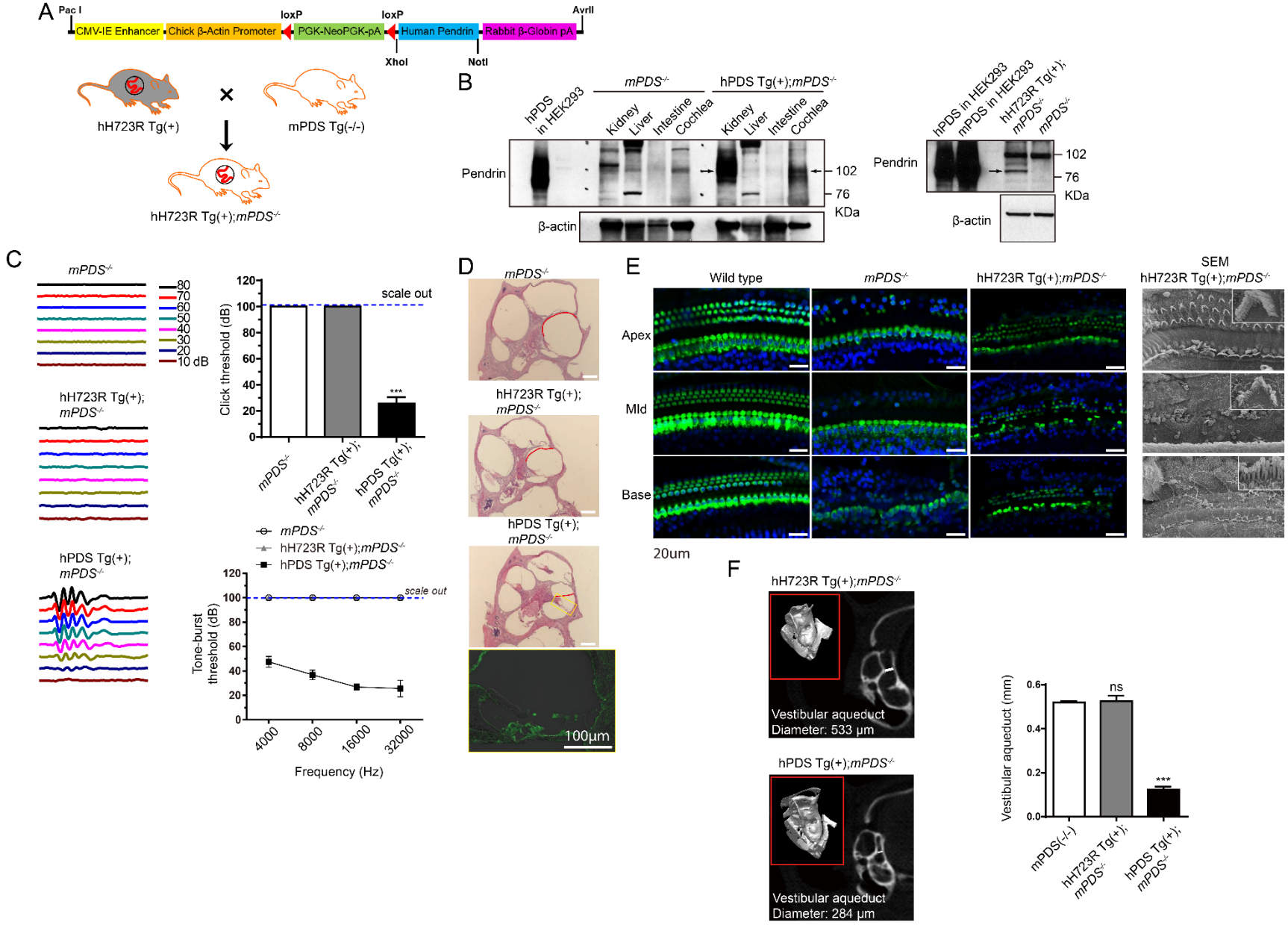
A
Pac I
loxP
loxP
AvrII
CMV-IE Enhancer
Chick β-Actin Promoter
PGK-NeoPGK-pA
Human Pendrin
Rabbit β-Globin pA
XhoI
NotI
hH723R Tg(+)
mPDS Tg(-/-)
hH723R Tg(+);mPDS-/-
B
hPDS in HEK293
mPDS-/-
hPDS Tg(+);mPDS-/-
Kidney
Liver
Intestine
Cochlea
Pendrin
β-actin
102
76
KDa
hPDS in HEK293
mPDS in HEK293
hH723R Tg(+); mPDS-/-
mPDS-/-
C
mPDS-/-
80
70
60
50
40
30
20
10 dB
hH723R Tg(+); mPDS-/-
hPDS Tg(+); mPDS-/-
Click threshold (dB)
scale out
***
mPDS-/-
hH723R Tg(+); mPDS-/-
hPDS Tg(+); mPDS-/-
mPDS-/-
hH723R Tg(+);mPDS-/-
hPDS Tg(+);mPDS-/-
Tone-burst threshold (dB)
scale out
4000
8000
16000
32000
Frequency (Hz)
D
mPDS-/-
hH723R Tg(+); mPDS-/-
hPDS Tg(+); mPDS-/-
100μm
E
Wild type
mPDS-/-
hH723R Tg(+);mPDS-/-
SEM
hH723R Tg(+);mPDS-/-
Apex
Mid
Base
20um
F
hH723R Tg(+);mPDS-/-
Vestibular aqueduct
Diameter: 533 μm
hPDS Tg(+);mPDS-/-
Vestibular aqueduct
Diameter: 284 μm
Vestibular aqueduct (mm)
ns
***
mPDS(-/-)
hH723R Tg(+); mPDS-/-
hPDS Tg(+); mPDS-/-

Figure S3. Generation of a human H723R-pendrin mouse model mimicking deafness in human DFNB4.

(A) Construct of the human p.H723R *SLC26A4* transgene in the pCB vector backbone. The wild-type (WT) or the p.H723R *SLC26A4* gene is Cre-inducible. The human WT-pendrin (hPDS) and H723R-pendrin (hH723R) transgenic mice [Tg(+)] were crossed with pendrin knock-out [$mPDS^{-/-}$] mice to generate hH723R Tg(+);$mPDS^{-/-}$ mice, in which only ectopic hH723R-pendrin was expressed without expression of mouse pendrin. To induce transgene expression in the inner ear, we crossed this strain with Pax2-Cre mice. (B) When WT- or hH723R-Tg(+) mice were crossed with Pax2-Cre, expression of the *SLC26A4* gene was observed in the inner ear and kidney (black arrows), but not in the other organs. (C) Auditory brainstem response by click and tone-burst stimuli for $mPDS^{-/-}$, hH723R(+);$mPDS^{-/-}$, and hPDS Tg(+);$mPDS^{-/-}$ mice. $mPDS^{-/-}$ and hH723R Tg(+);$mPDS^{-/-}$ mice were deaf, whereas the hearing function of hPDS Tg(+);$mPDS^{-/-}$ mice was nearly normalized (n = 8 mice in each group). (D) H&E staining of the inner ear showing that mPDS(−/−) and hH723R Tg(+);$mPDS^{-/-}$ mice had dilatation of the scala media, whereas hPDS Tg(+);$mPDS^{-/-}$ mice had normal sized scala media without endolymphatic hydrops. Immunostaining of the inner ear (lower panel) showed ectopic pendrin expression (anti-pendrin antibody, green) in the hair cells, supporting cells, inner limbus, lateral wall, and stria vascularis (Pax2-Cre-dependent). Scale bar, 20 μm. (E) Immunofluorescence and surface electron microscopy (SEM) images of the organ of Corti labeled with phalloidin (green) and DAPI (blue) in wild-type, $mPDS^{-/-}$, and hH723R Tg(+);$mPDS^{-/-}$ mice. Note that the outer hair cells showed better survival in hH723R Tg(+);$mPDS^{-/-}$ than in $mPDS^{-/-}$ mice. Magnification of electron microscope is x2000 [inset: x30000 (upper and middle), and x35000 (lower)). Scale bars, 20 μm. (F) Micro-computed tomogram was performed to compare the size of vestibular aqueduct. hH723R Tg(+);$mPDS^{-/-}$ mice had enlarged vestibular aqueduct, which was comparable to $mPDS^{-/-}$ mice. In contrast, hPDS Tg (+);$mPDS^{-/-}$ showed significantly normalized size of vestibular aqueduct when compared to that of $mPDS^{-/-}$ (n = 6–9 in each group). ns, not significant; ***, $p < 0.001$.